SIN-CHN
SCIENTIFIC PRESS PTE.LTD.

Molecular & Cellular Biomechanics 2024, 21(3), 518.
https://doi.org/10.62617/mcb518

Article

Numerical simulation of muscle force distribution during high-intensity athletic movements

Huaiyuan Deng

Life Science College, Sichuan University, Cheng Du 610065, China; denghuaiyuan@stu.scu.edu.cn

CITATION

Deng H. Numerical simulation of muscle force distribution during high-intensity athletic movements. Molecular & Cellular Biomechanics. 2024; 21(3): 518. https://doi.org/10.62617/mcb518

ARTICLE INFO

Received: 12 October 2024
Accepted: 21 October 2024
Available online: 6 December 2024

Abstract: Athletes performing high-intensity movements such as sprinting, jumping, and powerlifting rely on precise muscle coordination to generate the necessary forces for efficient movement. Examining how forces are distributed across muscle groups during these activities is critical for enhancing performance and reducing injury risks. However, detailed insights into the muscle force contributions during these specific movements are still limited. This study aims to address this gap by using advanced biomechanical techniques and numerical simulations to analyze the distribution of muscle forces in athletes engaged in these high-intensity tasks. Thirty-two athletes, including 15 professionals and 17 amateurs, participated in this research. Data were collected using motion capture systems, electromyography (EMG), and force plates. The musculoskeletal simulations were run on OpenSim, focusing on key muscle groups like the quadriceps, hamstrings, gluteus maximus, gastrocnemius, and iliopsoas. In sprinting, the quadriceps generated peak force during the stance phase, reaching 1452 N between 200–250 ms, while the gastrocnemius & soleus produced 845 N, contributing to ankle plantarflexion. The iliopsoas took over during the swing phase, peaking at 620 N to elevate the leg. In jumping, the quadriceps exhibited a maximum force of 1480 N in the take-off phase, with the gastrocnemius reaching 1020 N, supporting upward propulsion. During powerlifting, particularly the back squat, the quadriceps reached 1520 N during the concentric phase, while the hamstrings peaked at 1220 N, contributing to knee stabilization and hip extension.

Keywords: biomechanical techniques; motion capture systems; electromyography; precise muscle coordination; powerlifting; numerical simulations

1. Introduction

High-intensity athletic movements, such as sprinting, jumping, and powerlifting, place significant demands on the musculoskeletal system, requiring the coordinated effort of multiple muscle groups to produce the necessary forces for movement and stability [1,2]. Understanding how these forces are distributed across different muscles during these activities is crucial for optimizing athletic performance, preventing injuries, and improving training regimens [3,4]. Simulating muscle force distribution during these complex movements provides valuable insights into the biomechanics of athletic performance, allowing athletes, coaches, and sports scientists to tailor interventions more effectively [5,6].

The study of muscle force distribution is especially relevant in high-intensity sports because these activities typically involve rapid accelerations, decelerations, and changes in direction, which subject the body to high mechanical loads [7–9]. Athletes engaged in sprinting, jumping, and powerlifting often experience extreme forces through their lower limbs, hips, and core, with varying levels of involvement from muscles like the quadriceps, hamstrings, gastrocnemius, and gluteus maximus [10,11]. Moreover, upper body muscles such as the shoulders and erector spinae also contribute

significantly to balance, stability, and overall force production in powerlifting and certain phases of sprinting [12]. Investigating the distribution of forces across these muscle groups can help identify key moments during movement where peak forces occur, potentially leading to improved techniques and strategies to enhance performance and reduce injury risk [13].

Previous research has predominantly focused on muscle activation patterns and general biomechanics during high-intensity movements, but fewer studies have comprehensively examined the precise distribution of muscle forces using advanced simulation techniques [14–18]. By leveraging cutting-edge technologies such as motion capture, electromyography (EMG), and force plate analysis in combination with musculoskeletal modeling software, this study aims to provide a more detailed analysis of how forces are distributed among the primary muscle groups during high-intensity movements [19–20]. These simulations offer a unique opportunity to visualize and quantify muscle engagement, highlighting the most heavily loaded muscles during the key movement phases, including stance, take-off, and landing. This study uses numerical simulations to analyze muscle force distribution during high-intensity athletic activities, focusing specifically on three fundamental movements: sprinting, vertical jumping, and powerlifting. Each of these movements presents unique biomechanical challenges and requires different patterns of muscle activation and force generation. Sprinting involves rapid cyclic motion with alternating phases of propulsion and recovery while jumping requires explosive power and precise coordination of multiple joints for a successful take-off and controlled landing. On the other hand, powerlifting emphasizes maximum force production to move heavy weights, engaging a broad range of muscle groups in both the lower and upper body.

The proposed study uses numerical simulations to conduct a comprehensive analysis of muscle force distribution during high-intensity athletic movements. By focusing on three key movements—sprinting, vertical jumping, and powerlifting—this research will investigate how different muscle groups contribute to the generation, absorption, and transfer of forces throughout each movement cycle. The study will use advanced tools such as motion capture systems, electromyography (EMG), force plates, and musculoskeletal modeling software (OpenSim) to simulate muscle activity and force distribution in both professional and amateur athletes [21–25]. The proposed work will involve detailed data collection of movement patterns, muscle activation, and ground reaction forces, which will be processed and integrated into a customized musculoskeletal model. This model will then analyze joint kinematics, calculate joint moments, and estimate individual muscle forces. Furthermore, the study will compare the force distribution patterns between professional and amateur athletes, providing insights into biomechanical efficiency, performance optimization, and injury prevention. The findings from this research will have practical implications for designing more effective training programs and enhancing athletic performance, particularly in high-intensity sports [26–32].

The structure of the paper is organized as follows: Section 2 provides a comprehensive overview of the methodology, detailing the participant selection process, data collection techniques, and the musculoskeletal modeling approach used to simulate muscle force distribution. Section 3 presents an in-depth analysis of the findings, examining muscle engagement across different phases of high-intensity

movements such as sprinting, jumping, and powerlifting. Finally, Section 4 concludes the study, summarizing key insights and discussing the practical implications for athletic performance optimization and injury prevention.

2. Methodology

2.1. Participant selection

For the study, 32 athletes were selected, representing a diverse group, to ensure a comprehensive analysis of muscle force distribution. The selection process focused on recruiting participants who regularly engage in high-intensity sports, ensuring they possess the necessary physical conditioning and experience for the types of movements under analysis. Participants were drawn from two main categories: professional athletes (n = 15) and amateur athletes (n = 17). The professional athletes included individuals competing in sprinting, weightlifting, and competitive cycling at regional and national levels, with an average of 6.7 years of professional experience. The amateur athletes had an average of 4.2 years of regular training experience in high-intensity activities such as CrossFit, amateur powerlifting, and recreational athletics.

Regarding demographic details, the participants were 22 males and 10 females, ensuring gender representation for both groups. The age range of the participants was between 22 to 35 years, with a mean age of 27.4 years. All participants had a body mass index (BMI) within the 18.5 to 26.4 kg/m^2 range, falling into the healthy to athletic category, which was essential to standardize the biomechanical simulations and avoid variations due to extreme body mass or height differences. The average height of participants was 175.3 cm (range: 162 cm to 189 cm), and the average weight was 72.6 kg (range: 61.8 kg to 86.3 kg).

Inclusion criteria required all participants to have no history of major musculoskeletal injuries within the past 18 months, as injuries could significantly alter movement mechanics and muscle force distribution. Furthermore, participants were required to complete a movement proficiency screening, confirming their ability to perform the high-intensity athletic movements required for the study, such as maximal-effort sprints, vertical jumps, and powerlifting movements (squat, deadlift, clean).

2.2. Tools and techniques

Advanced biomechanical tools and computational techniques were employed to accurately simulate and analyze muscle force distribution during high-intensity athletic movements. The integration of motion capture technology, electromyography (EMG), force plates, and sophisticated numerical simulation software provided a robust framework for capturing and analyzing the complex dynamics of muscle activity. A 12-camera Vicon motion capture system was used to record the athletes' movements with high precision. This optical tracking system operates at a frequency of 250 Hz, ensuring that even rapid, high-intensity movements are captured in sufficient detail. The reflective markers were placed on key anatomical landmarks following the Plug-in Gait model to track joint angles and body segment movements.

The motion capture data allowed for the construction of accurate kinematic profiles of each athletic movement, forming the foundation for subsequent biomechanical analysis.

Surface electromyography (EMG) was employed to measure muscle activation patterns in real-time during the athletic movements. A Delsys Trigno wireless EMG system was utilized, with electrodes placed on the primary muscle groups involved in the selected movements, including the quadriceps, hamstrings, gluteus maximus, gastrocnemius, and erector spinae. The EMG data was sampled at 1000 Hz to capture fine details of muscle activation. This data provided insights into the timing and intensity of muscle engagement, which was critical for correlating muscle force with specific movement phases. Advanced Mechanical Technology, Inc. (AMTI) force plates were used to measure ground reaction forces (GRFs) during dynamic movements such as jumping, sprinting, and lifting to complement the motion capture and EMG data. The force plates were recorded at a sampling rate of 2000 Hz, ensuring precise capture of the force dynamics, especially during explosive actions. These GRF measurements were essential for calculating the external forces acting on the body, which were then used to compute internal muscle forces via inverse dynamics analysis.

OpenSim, a widely used musculoskeletal modeling software, was selected to simulate muscle force distribution. OpenSim enables the creation of detailed biomechanical models and the simulation of muscle forces during movement. A generic full-body musculoskeletal model with 39 degrees of freedom and 92 muscle actuators was customized based on participant-specific anthropometric data collected through the motion capture system. Inverse kinematics (IK) was used within OpenSim to calculate joint angles from the motion capture data. Subsequently, inverse dynamics (ID) calculations were performed to determine the net joint moments based on the measured ground reaction forces. Static optimization techniques were applied to estimate individual muscle forces, solving the distribution of muscle forces that produce the observed joint moments while minimizing total muscle activation.

All raw data, including motion capture, EMG, and force plate recordings, were synchronized and processed using matrix laboratory (MATLAB). Custom MATLAB scripts were developed to preprocess the data, including filtering the EMG signals with a fourth-order Butterworth filter (20–450 Hz bandpass) and smoothing motion capture data using a low-pass filter with a 6 Hz cutoff frequency to remove noise. After preprocessing, the data was fed into the OpenSim model, which was used to drive simulations of muscle force distribution. MATLAB was also used for statistical analysis of the simulation results, where muscle force outputs were compared across different movements and participant groups.

To ensure the accuracy of the numerical simulations, the results were validated by comparing the predicted muscle forces to known physiological parameters from the literature and cross-referencing the muscle activation patterns derived from the EMG data. This cross-validation helped confirm that the model's muscle force predictions were consistent with experimental measurements and established biomechanical knowledge. The results of the simulations, including muscle force distribution patterns and joint load profiles, were visualized using OpenSim's built-in visualization tools and custom plots generated in MATLAB. These visualizations provided clear insights into which muscle groups were most engaged during each movement phase and how

forces were distributed across the body. The following table provides the tools used in the study (**Table 1**).

Table 1. Tools and techniques employed in the study.

Tool/Technique	Purpose	Specifications	Data Collected
Vicon Motion Capture System	Capturing 3D kinematic data of body movements	12 cameras, 250 Hz frequency, Plug-in Gait model	Joint angles, body segment movements
Delsys Trigno Wireless EMG System	Recording muscle activation patterns during movement	Wireless electrodes, 1000 Hz sampling frequency	Muscle activation timings and intensities
AMTI Force Plates	Measuring ground reaction forces during dynamic movements	2000 Hz sampling rate	Ground reaction forces (GRFs)
OpenSim Software	Simulating muscle forces and biomechanical analysis	The full-body musculoskeletal model with 39 degrees of freedom, 92 muscle actuators	Muscle force distribution, joint moments
MATLAB (Data Processing)	Data preprocessing, synchronization, and statistical analysis	Custom scripts, filtering (Butterworth, low-pass), data synchronization	Filtered motion capture, EMG, and force plate data
Inverse Kinematics (OpenSim)	Calculating joint angles from motion capture data	Applied to motion capture data for kinematic modeling	Joint angles and body segment positioning
Inverse Dynamics (OpenSim)	Estimating net joint moments based on ground reaction forces	Used ground reaction forces to compute internal joint forces	Joint moments
Static Optimization (OpenSim)	Estimating individual muscle forces	Optimization technique to minimize muscle activation while reproducing joint moments	Individual muscle forces during movements
MATLAB (Visualization)	Visualizing muscle force distribution and analysis results	Custom plots and visualizations	Muscle force distribution patterns, joint loads
EMG Signal Processing	Filtering and analyzing muscle activation data	4th-order Butterworth filter (20–450 Hz bandpass)	Cleaned muscle activation data
Ground Reaction Force Analysis	Measuring external forces acting on the body during movements	Force plates, 2000 Hz sampling rate	External forces applied to lower limbs and body

2.3. Musculoskeletal model

The present study developed a detailed musculoskeletal model using OpenSim to simulate the muscle force distribution during high-intensity athletic movements. The model used for this study was a full-body musculoskeletal model that was customized for each participant based on their anthropometric measurements, ensuring accuracy in force and movement simulations. The musculoskeletal model contained 39 degrees of freedom (DOF), allowing for complex multi-joint movements, and included 92 muscle actuators representing the primary muscles involved in athletic movements.

Model Structure: The model was designed to replicate the human skeletal and muscular systems, with key joints and muscle groups specifically included to capture the dynamics of high-intensity movements. Each body segment was modeled as rigid bodies connected by joints, with the following joints being essential for the movements under study:

- Hip joint (3 DOF: flexion/extension, abduction/adduction, internal/external rotation)

- Knee joint (1 DOF: flexion/extension)
- The ankle joint (2 DOF: dorsiflexion/plantarflexion, inversion/eversion)

Multiple muscles actuated each of these joints, and the model included muscle-tendon units for each muscle, representing muscle fiber properties (e.g., length, velocity, and activation) and tendon elasticity. The muscle actuators within the model were modeled based on the Hill-type muscle model, which describes the muscle's force generation capacity through three key elements: the contractile element (representing active muscle fibers), the series elastic element (tendons), and the parallel elastic element (passive muscle components).

Muscle Parameter Customization: To enhance the model's fidelity, muscle parameters were individualized for each participant based on their specific height, weight, and limb lengths. This involved scaling the generic OpenSim model using participant-specific anthropometric data collected through the motion capture system. The scaling process ensured that muscle lengths, moment arms, and force-generation properties accurately reflected the participants' physiological structures.

The following muscle parameters were customized:

- Maximum isometric force for each muscle group, adjusted based on body mass and size.
- Optimal muscle fiber and tendon slack length ensure the model replicates muscle function across various joint angles.
- The rotation angle of muscle fibers affects the force transfer from the muscle to the tendon.

Muscle Activation and Force Production: The musculoskeletal model used muscle activation patterns obtained from the EMG data to drive the simulation of muscle forces. The relationship between neural activation and muscle force was modeled using a dynamic activation-deactivation model, accounting for the time it takes for muscles to reach full activation or relaxation. The Hill-type muscle model incorporated these activation dynamics to simulate realistic muscle force production during rapid, high-intensity movements.

Inverse dynamics was employed to calculate the forces produced by individual muscles, whereby motion capture and force plate data were used to compute joint moments. These joint moments were then resolved into individual muscle forces using static optimization. This optimization method minimized the sum of squared muscle activations, a commonly used criterion in biomechanics to estimate physiologically realistic muscle forces. By doing so, the model could distribute the required joint moments across the contributing muscles based on their capacity to generate force.

Consideration of Muscle Fatigue: One important aspect of the model was the consideration of muscle fatigue, particularly during prolonged or repetitive high-intensity movements. While the base OpenSim model does not inherently simulate muscle fatigue, the study incorporated an empirical model that adjusted muscle force capacity over time based on known fatigue parameters from the literature. This adjustment allowed for more accurate simulation of movements like sprints or weightlifting sets, where muscle performance decreases as fatigue sets in.

Joint Stability and Force Distribution: The model also accounted for joint stability by ensuring that muscles were appropriately co-activated to stabilize joints during high-intensity movements. For example, during the simulation of sprinting,

muscles around the knee, such as the quadriceps and hamstrings, were co-activated to ensure stability under high loads. The model distributed forces between these muscle groups in a manner that maintained joint stability while optimizing the overall force generation for movement.

Validation of the Musculoskeletal Model: To validate the accuracy of the musculoskeletal model, the simulated muscle forces were compared against experimental data, including EMG readings and known force production capacities from the literature. Additionally, the joint angles and moments predicted by the model were validated against the motion capture data to ensure that the model accurately reproduced the participants' movements. This validation process was crucial to ensure that the simulation results could be considered reliable for further analysis.

Limitations and Assumptions: While the musculoskeletal model provided detailed insights into muscle force distribution, several assumptions were made that could influence the results. For instance, the static optimization method assumes that muscles minimize overall activation, which may not fully capture the complex neural strategies employed during high-intensity movements. Additionally, the Hill-type muscle model used in this study simplifies muscle-tendon interactions, and further refinement of tendon elasticity and force-velocity relationships could enhance the model's precision.

2.4. Experimental design

The experimental design of this study was carefully crafted to simulate and analyze muscle force distribution during high-intensity athletic movements, ensuring that the data collected accurately reflects real-world conditions. The design integrated experimental data collection and computational modeling to understand the biomechanics involved comprehensively. This section details the experimental procedures, equipment setup, and data acquisition protocols used to obtain the necessary inputs for the musculoskeletal simulations.

Participant Preparation and Warm-Up: Before data collection, all participants underwent a standardized warm-up session to ensure they were physically prepared for the high-intensity movements required in the experiment. The warm-up included 10 min of light aerobic activity, followed by dynamic stretching and movement-specific drills to engage the muscles most involved in the experimental tasks. This was essential to prevent injury during the trials and ensure consistent participant muscle performance.

Experimental Task Selection: The tasks selected for the study were chosen based on their ability to represent a wide range of high-intensity athletic movements commonly observed in sports and fitness settings.

Three distinct movements were selected:

1) Maximal sprinting: Participants performed three 30-meter sprints at maximal effort, focusing on the explosive use of lower body muscles.
2) Vertical jumping: Participants completed five maximal vertical jumps, using the arms for momentum while focusing on the lower body muscle groups.
3) Powerlifting movements: Participants performed two major powerlifting exercises:

- Back Squat (3 repetitions at 85% of their one-repetition maximum)
- Deadlift (3 repetitions at 85% of their one-repetition maximum)

These movements were selected because they engage multiple muscle groups and joints in dynamic, high-intensity ways, providing a varied dataset for simulating muscle force distribution across different types of athletic exertion.

2.5. Data collection setup

The experimental setup involved using several high-precision instruments to simultaneously capture motion, muscle activity, and ground reaction forces. Each participant performed the movements in a controlled laboratory environment equipped with the following tools:

- Vicon motion capture system: A 12-camera system was used to capture 3D kinematic data, with reflective markers placed at key anatomical landmarks based on the Plug-in Gait model. The motion capture system recorded at 250 Hz, providing high-resolution data on joint angles, segment velocities, and accelerations.
- Electromyography (EMG): Surface EMG electrodes were applied to major muscle groups involved in the selected movements. EMG data was collected at 1000 Hz, providing detailed information on muscle activation levels during each movement phase. The primary muscles monitored included the quadriceps, hamstrings, gluteus maximus, gastrocnemius, erector spine, biceps femoris, and rectus abdominis.
- Force plates: AMTI force plates were used to measure ground reaction forces during each movement, with a sampling rate of 2000 Hz. These plates were essential for capturing the dynamic forces exerted by the athletes during jumping, sprinting, and powerlifting, allowing for the calculation of net joint forces and torques.

2.6. Trial execution and data recording

Each participant performed the selected movements under the supervision of trained researchers to ensure proper form and execution. The order of the tasks was randomized to minimize any order effects that could influence muscle performance due to fatigue. Five trials were conducted for each movement, with adequate rest periods of 3–5 min between each trial to allow muscle recovery and prevent fatigue from affecting the results. Data from the motion capture system, EMG, and force plates were collected and synchronized for each movement. This synchronized data was crucial for accurately mapping the muscle forces to the corresponding phases of movement, such as the stance and swing phases of sprinting or the eccentric and concentric phases of lifting.

Control Variables: To ensure the reliability and validity of the experiment, several control variables were carefully maintained:

- Footwear: Participants wore standardized athletic footwear to minimize ground contact forces and lower limb mechanics variability.
- Surface: All movements were performed on a level surface to control for variations in ground reaction forces due to surface incline or texture.

- Environmental conditions: The laboratory environment was kept at a consistent temperature of 22 ℃, and humidity levels were monitored to ensure they remained constant. This prevented external environmental factors from influencing muscle performance.

Following the data collection, all raw data were processed using MATLAB for initial cleaning and synchronization. EMG signals were filtered using a fourth-order Butterworth filter (20–450 Hz) to remove noise, and motion capture data were smoothed using a low-pass filter (cutoff frequency: 6 Hz) to eliminate any unwanted high-frequency noise. The cleaned data was input for the OpenSim musculoskeletal model (**Figure 1**), which simulated the muscle force distribution during each movement. The data processing step also included the extraction of relevant joint kinematics, ground reaction forces, and muscle activation levels, which were used to drive the numerical simulations.

To improve the robustness of the findings, each participant repeated the experimental tasks multiple times (five trials per movement), and the order of tasks was randomized across participants. Randomization was used to ensure that any variability in muscle performance or fatigue effects were evenly distributed across the different movements and trials. The experimental design adhered to all ethical standards for human subject research. Before participation, each athlete provided informed consent, acknowledging their understanding of the risks and voluntary participation in the study. The university's ethics review board approved the study protocol, and safety measures were implemented to address any potential injuries during high-intensity tasks. Athletes were monitored throughout the trials, and any discomfort or fatigue was addressed immediately to ensure participant well-being.

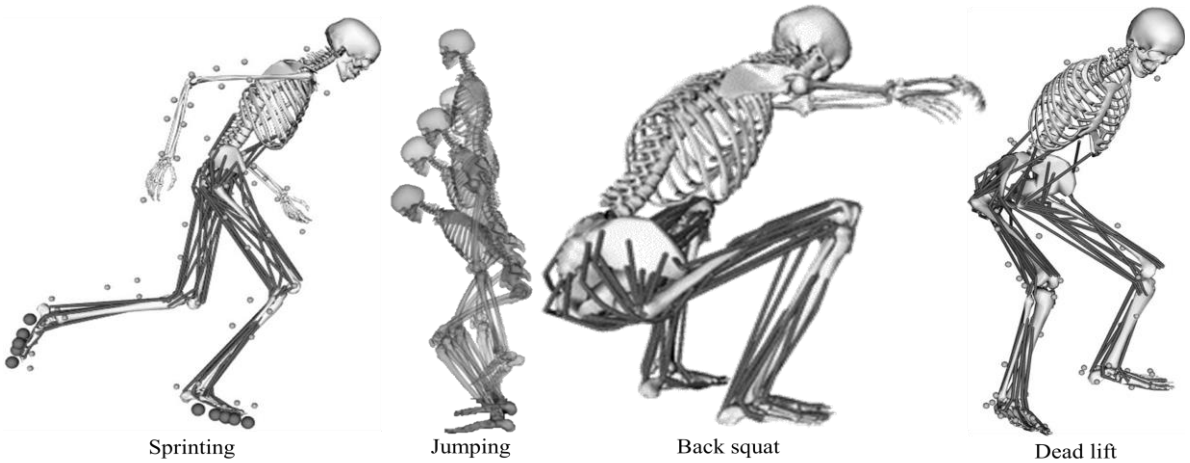

Figure 1. Musculoskeletal model.

3. Result analysis

3.1. Force distribution analysis

i) Force distribution analysis for sprinting:

The force distribution analysis for sprinting, as shown in **Figure 2**, reveals key insights into how different muscle groups contribute to movement across the stance and swing phases of the sprinting cycle. The primary muscles analyzed include the

quadriceps, gastrocnemius & soleus, hamstrings, and iliopsoas, with distinct patterns of engagement observed during each phase.

- Stance Phase (0–500 ms): During the stance phase, where the foot is in contact with the ground, there is a progressive increase in force production across all major muscle groups. The quadriceps dominate, reaching their peak force of 1452 N between 200–250 ms when the body pushes off the ground. This substantial force is crucial for extending the knee and generating forward propulsion. Following this, the quadriceps force begins to decline as the foot transitions towards the end of the stance phase. Similarly, the gastrocnemius & soleus muscles, which are responsible for ankle plantarflexion, show a gradual increase in force, peaking at 845 N during the same 200–250 ms window. This highlights the importance of ankle extension in the push-off phase, contributing significantly to propulsion. The hamstrings also contribute significantly during the stance phase, especially between 150–200 ms, generating a peak force of 1023 N. The hamstrings aid in knee stabilization and hip extension, which is essential for maintaining stability and power during ground contact. As the stance phase progresses, the forces in all muscle groups gradually decrease, particularly in the final 450–500 ms window, where the body prepares to transition into the swing phase.
- Swing phase (500–800 ms): During the swing phase, where the foot is no longer in contact with the ground, there is a notable shift in muscle engagement. The primary hip flexor, the iliopsoas, becomes the dominant muscle, as it is responsible for lifting the leg and preparing it for the next stance phase. The iliopsoas force peaks at 620 N between 600–650 ms, indicating its crucial role in bringing the thigh forward. The hamstrings remain active during the late swing phase, particularly between 650–700 ms, generating 489 N of force. This force is critical in controlling leg deceleration and preparing for the upcoming ground contact. Throughout the swing phase, the quadriceps, gastrocnemius, and soleus are minimally engaged, as their role is limited while the leg is off the ground. The focus shifts entirely to the iliopsoas and hamstrings, which manage leg movement and positioning.

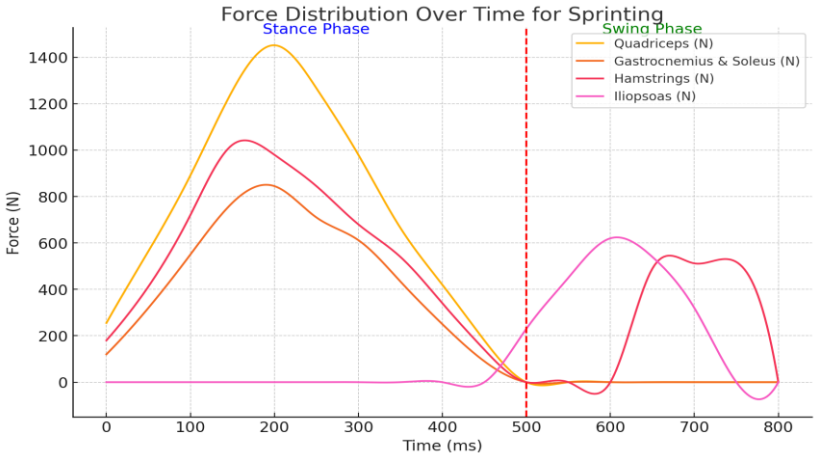

Figure 2. Force distribution for sprinting.

ii) Force distribution against time for the jumping activity:

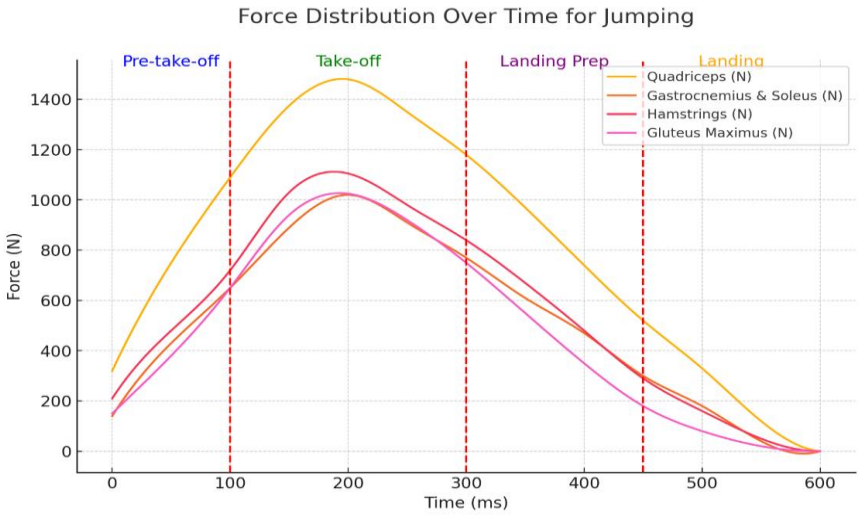

Figure 3. Force distribution for Jumping.

The data presented in **Figure 3** provides a comprehensive analysis of the force distribution among the primary muscles involved in the jumping activity, including the quadriceps, gastrocnemius & soleus, hamstrings, and gluteus maximus, across various phases of the jump: pre-take-off, take-off, landing preparation, and landing.

- Pre-Take-off Phase (0–100 ms): During the pre-take-off phase, the body prepares for the explosive jump by generating increasing force in the quadriceps, gastrocnemius & soleus, hamstrings, and gluteus maximus. The quadriceps, responsible for knee extension, start generating force at 320 N and rise sharply to 750 N between 50–100 ms, preparing the legs for the powerful extension that follows in the take-off phase. The gastrocnemius and soleus muscles also show a significant force increase from 140 N to 430 N during the pre-take-off phase, aiding ankle plantarflexion and assisting with the initial drive upward. The hamstrings and gluteus maximus, which contribute to hip extension and stabilization of the posterior chain, show similar force generation patterns, with the hamstrings rising from 210 N to 480 N and the gluteus maximus increasing from 150 N to 380 N.
- Take-off Phase (100–300 ms): The take-off phase is where the body generates maximum force to propel itself off the ground. The quadriceps exhibit the highest force during this phase, peaking at 1480 N between 200–250 ms, emphasizing their critical role in knee extension and the explosive upward movement of the jump. The gastrocnemius and soleus muscles show a similar pattern, with force increasing to 1020 N at the peak take-off phase, providing the necessary ankle extension for a powerful push-off. The hamstrings also play an essential role in stabilizing the knee and aiding in hip extension, peaking at 1105 N. The gluteus maximus, crucial for hip extension, generates a peak force of 1025 N at 200–250 ms. This muscle contributes significantly to the upward propulsion, working with the quadriceps and hamstrings to lift the body off the ground.
- Landing Preparation (300–400 ms): As the body prepares for landing, the forces in all muscle groups begin to decrease. The quadriceps reduce from 1350 N at

250–300 ms to 1180 N at 300–350 ms as the body shifts from propelling upward to controlling the descent. The gastrocnemius and soleus, responsible for absorbing some of the impact during landing, decline from 910 N to 770 N over this period. The hamstrings and gluteus maximus also reduce force output, transitioning from active take-off engagement to a stabilizing role during the descent. The hamstrings decrease to 840 N, while the gluteus maximus lowers to 750 N during landing preparation.

- Landing Phase (400–600 ms): During the landing phase, the forces in all muscle groups continue to decrease as the body absorbs the impact of the ground. The quadriceps gradually reduce force from 740 N during the initial landing (400–450 ms) to 120 N during the final landing (550–600 ms). This highlights the quadriceps' key role in controlling the landing by decelerating the body's downward momentum and stabilizing the knees. The gastrocnemius and soleus muscles, which aid shock absorption during ankle dorsiflexion, reduce from 470 N to 40 N by the final landing phase. Similarly, the hamstrings and gluteus maximus forces decrease, reflecting their reduced role as the body absorbs the impact and transitions into a stabilized position.

iii) Force distribution results for power lifting:

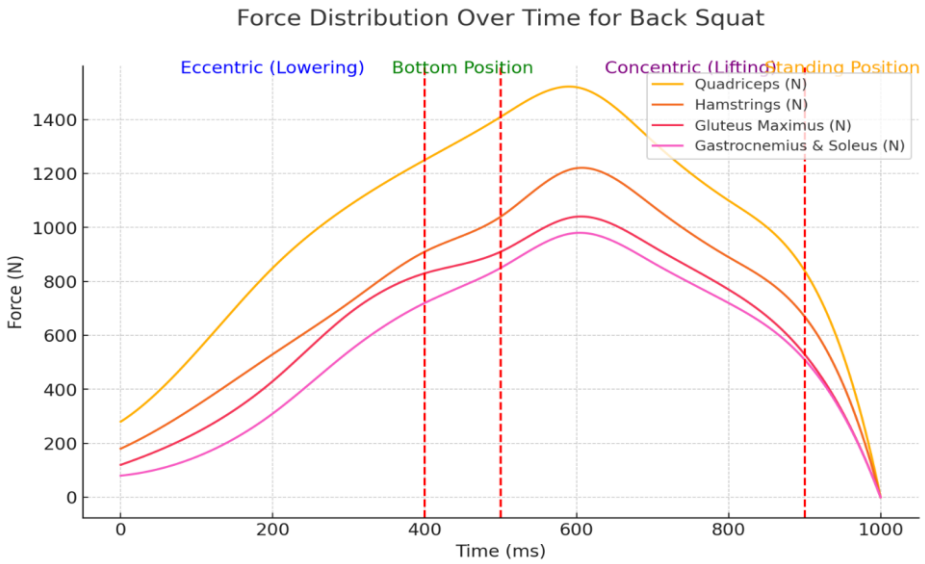

Figure 4. Back squat force distribution.

Figure 4 for the back squat highlights the involvement of the movement's quadriceps, hamstrings, gluteus maximus, and gastrocnemius & soleus muscles during both the eccentric (lowering) and concentric (lifting) phases.

- Eccentric Phase (0–400 ms): During the eccentric phase, as the lifter lowers into the squat position, all muscle groups show a progressive increase in force output as the body resists the gravitational pull. The quadriceps are the dominant force producers, starting at 280 N and rising to 1080 N by 300–400 ms, as they control knee flexion during the descent. This indicates the quadriceps' crucial role in stabilizing and controlling the descent. The hamstrings and gluteus maximus work together to control hip flexion during the eccentric phase, with the hamstrings increasing from 180 N to 720 N and the gluteus maximus increasing

from 120 N to 680 N by 300–400 ms. These posterior chain muscles help stabilize the hips and provide the necessary control over the squat descent. The gastrocnemius and soleus muscles provide additional stability at the ankles, increasing from 80 N to 540 N by 300–400 ms, helping to control the foot and lower leg position as the body descends into the bottom position.

- Bottom Position (400–500 ms): At the bottom of the squat, force output peaks across all muscle groups, with the quadriceps reaching 1250 N, the hamstrings at 910 N, and the gluteus maximus at 830 N. The gastrocnemius and soleus muscles reach 720 N, highlighting their role in maintaining balance and readiness for the concentric phase.
- Concentric Phase (500–1000 ms): As the lifter moves upward in the concentric phase, all muscles increase their force output to drive the body back to the standing position. The quadriceps reach their maximum force output of 1520 N between 600–700 ms, reflecting their critical role in extending the knees during the lift. The hamstrings and gluteus maximus also contribute significantly during the concentric phase, with the hamstrings peaking at 1220 N and the gluteus maximus at 1040 N. These muscles are essential for extending the hips and stabilizing the lower body during the upward movement. The gastrocnemius and soleus support ankle stability, peaking at 980 N during the 600–700 ms period. As the lifter approaches the standing position, all muscle forces gradually decrease.

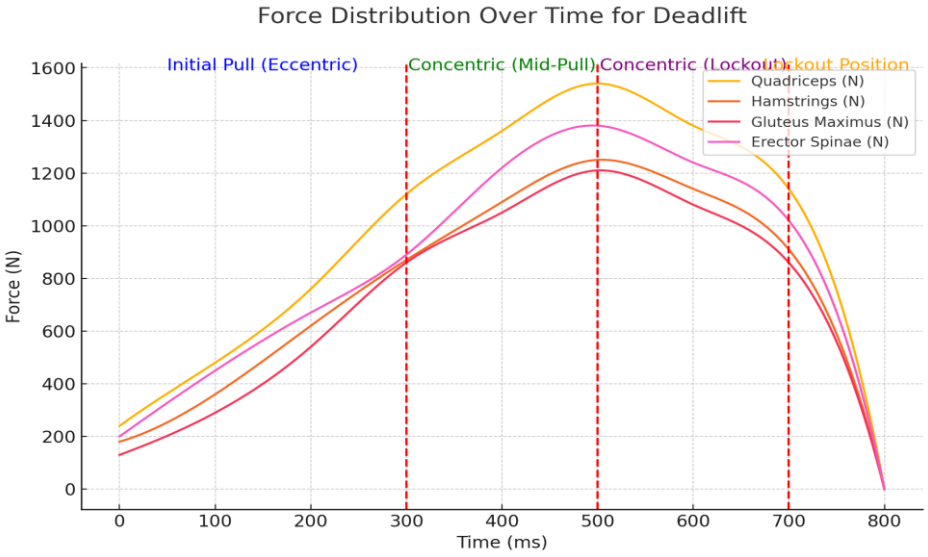

Figure 5. Deadlift force distribution.

In the deadlift (**Figure 5**), the force distribution highlights the roles of the quadriceps, hamstrings, gluteus maximus, and erector spine during the lift. The erector spinae plays a significant role in maintaining spinal stability and controlling the position of the upper body.

- Eccentric Phase (0–300 ms): During the initial pull in the eccentric phase, the quadriceps provide the primary force for knee extension, starting at 240 N and rising to 760 N by 200–300 ms. The quadriceps' role is to drive the initial pull of the bar off the ground. The hamstrings and gluteus maximus work in unison to

extend the hips, with the hamstrings increasing from 180 N to 620 N and the gluteus maximus increasing from 130 N to 540 N during the initial pull. These posterior muscles play a critical role in hip extension, which is necessary to initiate the movement. The erector spinae shows a significant increase in force, from 200 N to 670 N, as it stabilizes the spine and supports the upper body during the initial stages of the lift.

- Concentric Phase (300–800 ms): During the mid-pull and lockout phases, the quadriceps generate force, peaking at 1360 N during 400–500 ms. This force is essential for extending the knees and lifting the weight to the standing position. The hamstrings and gluteus maximus also peak during the concentric phase, with the hamstrings reaching 1250 N and the gluteus maximus reaching 1210 N at 500–600 ms. These muscles are critical for hip extension and play a key role in the lifter's ability to pull the bar past the knees and lockout at the top of the lift. The erector spinae shows the highest force production during the lockout phase, peaking at 1380 N, as it maintains spinal extension and prevents back rounding. This is vital for protecting the lower back during heavy lifting.

3.2. Kinematic analysis

i) Kinematic analysis for sprint cycle:

As shown in **Figure 6**, During the early stance (0–100 ms), the hip shows an increasing joint angle from 5.6° to 15.4°, with the angular velocity and acceleration peaking at 220°/s and 410°/s^2 in mid stance (100–150 ms). The hip reaches a maximum joint angle of 28.4° before decreasing during push-off and transitioning to the swing phase, where it reaches −20.1° during late swing (450–500 ms). The knee angle increases rapidly from 15.8° in early stance to a peak of 45.2° during mid stance. The angular velocity and acceleration peak at 380°/s and 600°/s^2 in mid-stance, decreasing gradually as the knee approaches late swing with a joint angle of −10.8°.

The ankle exhibits dorsiflexion during early stance with an angle of −2.3° and transitions to plantarflexion, peaking at 15.1° during late stance. The angular velocity peaks at 180°/s during late stance before decreasing into the swing phase, with the ankle reaching −15.8° by late swing. The shoulder starts with flexion during the arm forward swing, peaking at 65.4° during 100-150 ms. As the arms transition into a backward swing, the shoulder begins extending, reaching 25.3° by 250–300 ms. The elbow follows a similar pattern, peaking at 75.2° flexion during 350–400 ms, then extending during the arm backward swing with a joint angle of 25.3° by 450–500 ms.

ii) Kinematic Analysis for Jumping:

As shown in **Figure 7**, in the pre-take-off phase (0-100 ms), the hip joint angle increases from 10.2° to 22.5°, with a peak angular velocity of 100°/s and angular acceleration of 200°/s^2, showing preparation for the explosive jump. The knee also shows a sharp increase in joint angle from 20.5° to 35.0°, while the ankle transitions from dorsiflexion to plantarflexion, with an angle increasing from −5.0° to 2.5°. During the take-off phase (100–250 ms), the hip reaches a maximum joint angle of 45.0° and peaks in angular velocity at 180°/s during 150–200 ms. Similarly, the knee angle reaches 60.5° with a peak angular velocity of 220°/s during 150–200 ms. The

ankle exhibits significant plantarflexion, reaching 25.0° with an angular velocity peaking at 180°/s during the take-off phase.

In the flight phase (300–500 ms), the hip joint starts to flex, decreasing from 18.4° to −20.1°, while the knee reduces from 25.0° to −12.0°, and the ankle shows further dorsiflexion, reaching −25.0°. Angular velocities and accelerations decrease as the body reaches the peak of the jump. In the landing preparation and landing phases (500–800 ms), the hip angle shifts from −18.9° during flight to 12.0° during landing. The knee prepares for landing with a joint angle of 6.0° during 650–700 ms, while the ankle shifts from −28.0° during flight to 14.0° in the final landing, showing gradual plantarflexion. Angular velocities and accelerations stabilize as the body absorbs impact. For the shoulder, during the pre-take-off phase (0–100 ms), the shoulder joint flexes from 45.5° to 60.2° with a peak angular velocity of 160°/s during 100–150 ms. In the arm swing during take-off (150–250 ms), the shoulder transitions into extension, decreasing from 65.0° to 50.3°. The elbow moves through flexion in the pre-take-off phase, peaking at 75.0° at 0–50 ms and extending during the take-off and arm return phases.

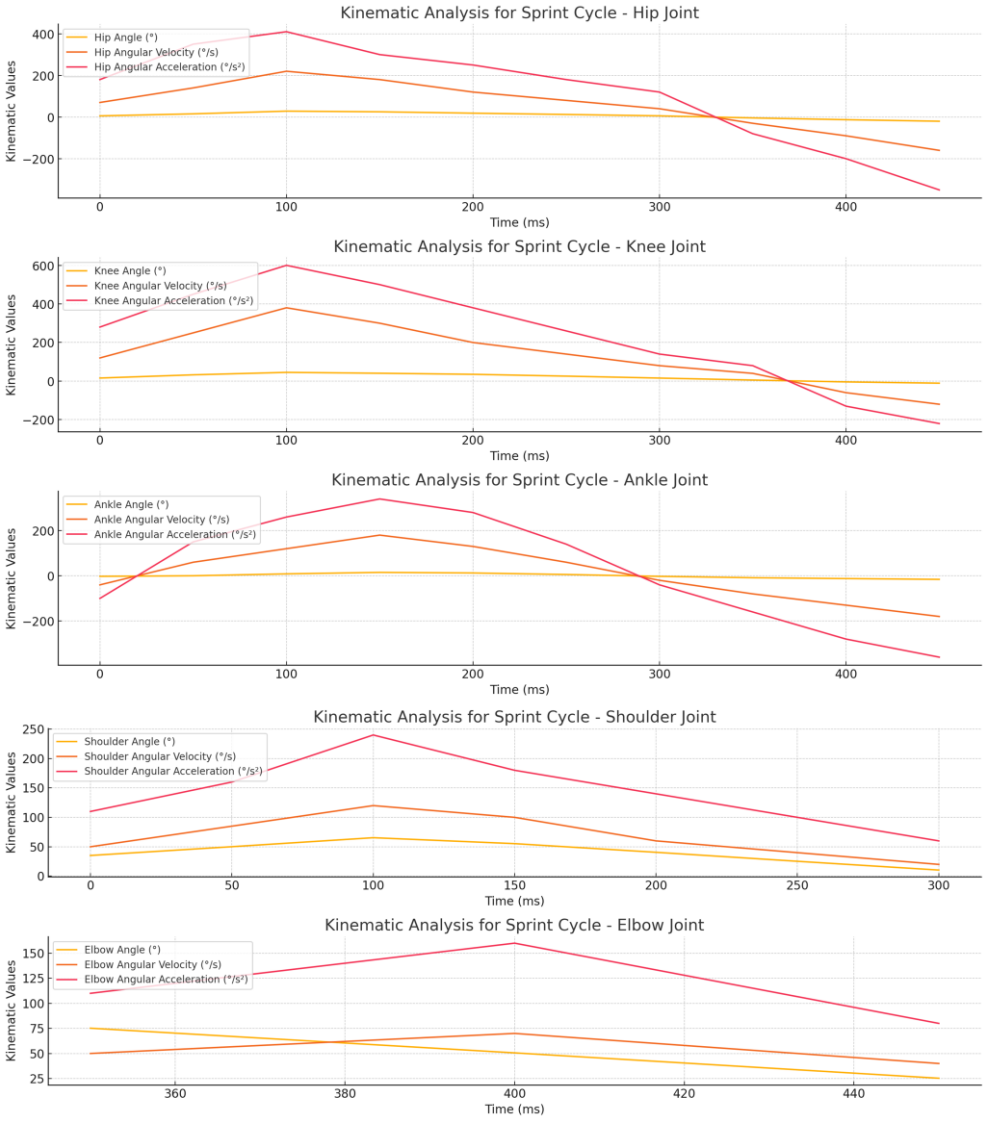

Figure 6. Kinematic analysis for sprint cycle.

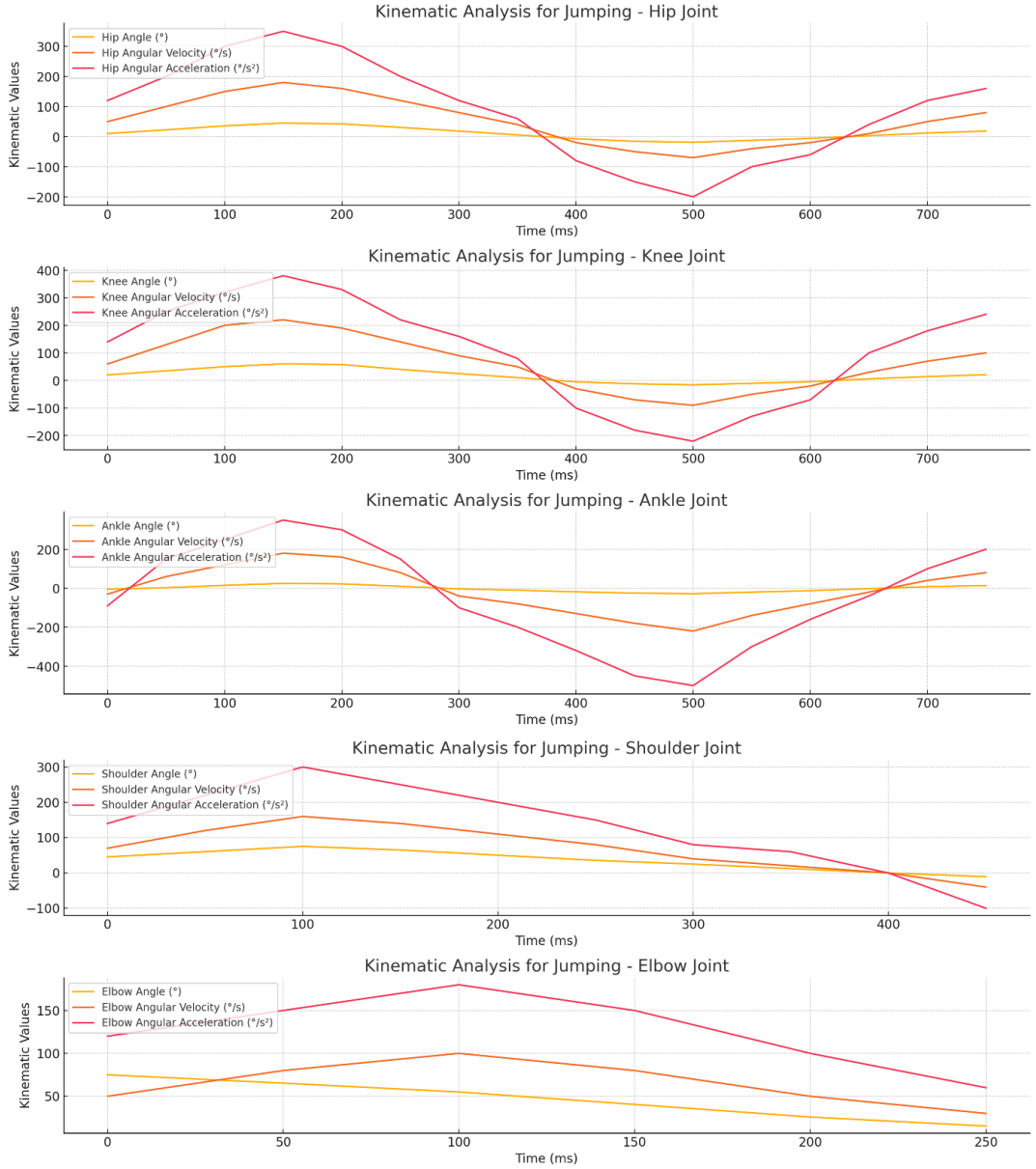

Figure 7. Kinematic analysis for Jumping.

iii) Kinematic analysis for powerlifting:

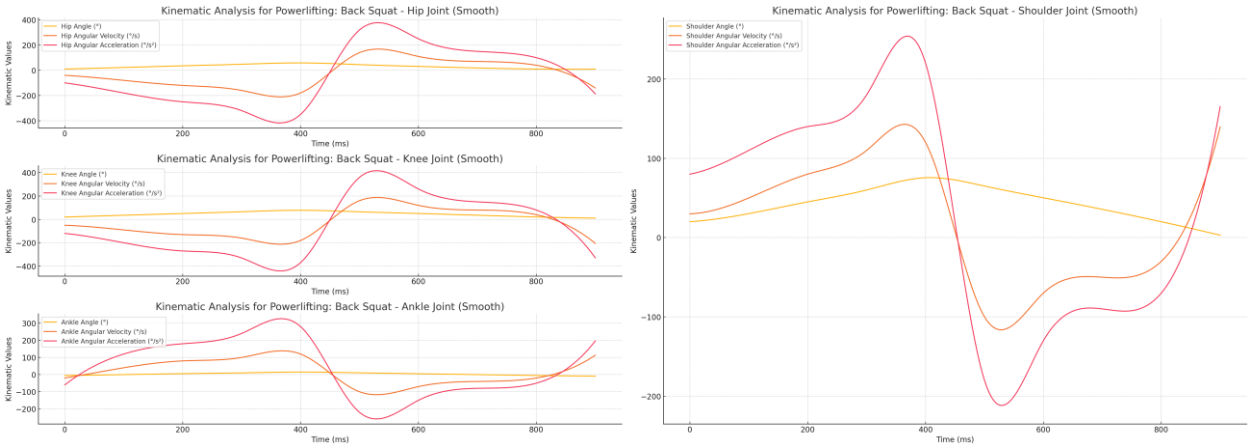

Figure 8. Kinematic analysis for powerlifting (back squat).

As shown in **Figure 8**, in the eccentric phase (lowering) of the back squat, the hip joint angle increases from 10.0° to 58.5° between 0–500 ms, with the angular velocity reaching −180°/s and the angular acceleration peaking at −350°/s^2 during the bottom position. The knee joint follows a similar pattern, increasing from 20.2° to 78.0°, while the ankle joint moves from −5.0° dorsiflexion to 15.0° plantarflexion, showing the transition from lowering to the bottom squat position. In the concentric phase (lifting) from 500–900 ms, the hip joint decreases from 58.5° to 10.0°, and the angular velocity reverses to 140°/s, peaking at 500–600 ms. The knee follows the same pattern, with the angle reducing from 78.0° to 20.8° and the ankle returning to −5.0° dorsiflexion by the end of the lift. The shoulder flexes during the eccentric phase, moving from 20.0° to 75.5° at 400–500 ms. During the concentric phase, the shoulder extends from 65.0° to 20.0°, with a peak angular velocity of −100°/s between 500–600 ms, stabilizing the upper body and maintaining posture throughout the lift.

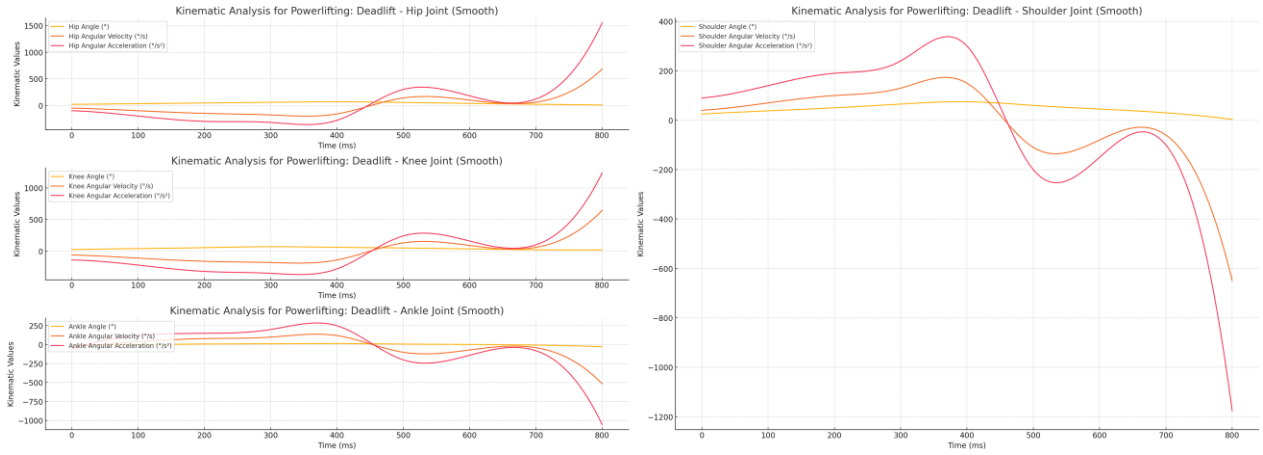

Figure 9. Kinematic Analysis for Powerlifting (deadlift).

As shown in **Figure 9**, In the initial pull phase (0–300 ms), the hip joint angle increases from 20.0° to 45.6°, with a peak angular velocity of −150°/s at 200–300 ms and an angular acceleration of −300°/s^2, indicating controlled hip extension. The knee joint follows a similar pattern, increasing from 25.5° to 55.1°, while the ankle moves from −5.0° dorsiflexion to 8.5° plantarflexion during the mid-pull phase, contributing to the overall lift. During the mid-pull (300–500 ms), the hip angle increases to 68.0°, with an angular velocity peaking at −180°/s before reversing in the concentric phase. The knee angle increases to 70.3°, while the ankle reaches 14.5° in plantarflexion, providing stability as the bar passes the knees. In the concentric lockout phase (500–800 ms), the hip joint decreases from 68.0° to 22.0°, and the angular velocity shifts to 140°/s, peaking between 500–600 ms. The knee and ankle angles similarly decrease, with the knee moving from 70.3° to 22.5° and the ankle returning to −5.0° dorsiflexion by the lockout position at 700–800 ms. The shoulder begins in flexion during the initial pull, increasing from 25.0° to 75.0° by 400–500 ms, reaching its peak flexion during the mid-pull. During the concentric phase, the shoulder moves into extension, decreasing to 30.0° by 700–800 ms as the lifter locks out the movement.

4. Conclusion and future work

This study provided an in-depth analysis of muscle force distribution during high-intensity athletic movements, specifically sprinting, jumping, and powerlifting. Using a combination of motion capture, EMG, force plates, and musculoskeletal modeling software, we could quantify the contribution of key muscle groups during various phases of these movements. The results showed that the quadriceps, hamstrings, gastrocnemius, and iliopsoas muscles played pivotal roles in generating and controlling forces across all movements, with notable differences in force production between the stance and swing phases in sprinting, the take-off and landing phases in jumping, and the eccentric and concentric phases in powerlifting. A key finding was the more efficient force distribution exhibited by professional athletes compared to amateurs, particularly in their ability to maintain joint stability under high loads. This difference highlights the importance of biomechanical efficiency in athletic performance and suggests that targeted training interventions can help improve amateur athletes' muscle engagement and movement efficiency. The insights gained from this study have practical implications for optimizing training programs in high-intensity sports. By understanding how different muscle groups contribute to force production, coaches and trainers can design more effective strength and conditioning programs to improve specific muscle performance and reduce injury risks.

Additionally, simulating and predicting muscle forces through musculoskeletal modeling offers a powerful tool for biomechanical research and athletic performance analysis.

Ethical approval: Not applicable.

Conflict of interest: The author declares no conflict of interest.

References

1. Kaya Utlu, D. (2023). Description, Types, and Prescription of the Exercise. In Functional Exercise Anatomy and Physiology for Physiotherapists (pp. 3-18). Cham: Springer International Publishing.
2. Stoppani, J. (2023). Jim Stoppani's encyclopedia of muscle & strength. Human Kinetics.
3. Schneider, I. (2024). Strength and Conditioning: Principles for Developing Peak Athletic Performance. Revista de Psicología del Deporte (Journal of Sport Psychology), 33(2), 292-300.
4. Cooley, A., & Pelot, T. Structure-Function Relationships of Tendons: Implications for Athletic Performance, Injury Prevention, and Rehabilitation Strategies.
5. McErlain-Naylor, S. A., King, M. A., & Felton, P. J. (2021). A review of forward-dynamics simulation models for predicting optimal technique in maximal effort sporting movements. Applied Sciences, 11(4), 1450.
6. Brewer, C. (2017). Athletic movement skills: Training for sports performance. Human Kinetics.
7. Silva, H. F. R. D. (2023). The role of acceleration and deceleration in agility, change of direction speed, and running in soccer players' movements.
8. Marvin, L., Read, P., McLean, B., Palmer, S., & Fransen, J. (2024). Training Interventions for Improved Deceleration Ability in Adult Team-Based Field Sports Athletes: A SYSTEMATIC REVIEW and META-ANALYSIS of the Literature. International Journal of Strength and Conditioning, 4(1).
9. Bustamante-Garrido, A., Izquierdo, M., Miarka, B., Cuartero-Navarrete, A., Pérez-Contreras, J., Aedo-Muñoz, E., & Cerda-Kohler, H. (2023). Mechanical Determinants of Sprinting and Change of Direction in Elite Female Field Hockey Players. Sensors, 23(18), 7663.
10. Ngo, D., & Kazmi, M. (2024). Power and strength training plan for off and on season for teenage runners.

11. Mulvey, M. (2024). Exertional Compartment Syndrome and the Development of Preventative Measures.
12. Arrenega, C. T. (2024). Effects of six weeks of squat training in the load-velocity profile of the squat and the deadlift (Doctoral dissertation).
13. Knudson, D. V. (2013). Qualitative diagnosis of human movement: improving performance in sport and exercise. Human kinetics.
14. Huygaerts, S., Cos, F., Cohen, D. D., Calleja-González, J., Guitart, M., Blazevich, A. J., & Alcaraz, P. E. (2020). Mechanisms of hamstring strain injury: interactions between fatigue, muscle activation and function. Sports, 8(5), 65.
15. Van Hooren, B., Teratsias, P., & Hodson-Tole, E. F. (2020). Ultrasound imaging to assess skeletal muscle architecture during movements: a systematic review of methods, reliability, and challenges. Journal of Applied Physiology, 128(4), 978-999.
16. Stessens, L., Gielen, J., Meeusen, R., & Aerts, J. M. (2024). Physical performance estimation in practice: A systematic review of advancements in performance prediction and modeling in cycling. International Journal of Sports Science & Coaching, 17479541241262385.
17. Frank, B. S. (2016). The influence of movement profile on the female athlete's biomechanical resilience & training load response to controlled exercise exposure (Doctoral dissertation, The University of North Carolina at Chapel Hill).
18. Li, K., Zhang, J., Wang, L., Zhang, M., Li, J., & Bao, S. (2020). A review of the key technologies for sEMG-based human-robot interaction systems. Biomedical Signal Processing and Control, 62, 102074.
19. S. Sudhakar and S. Chenthur Pandian, (2016), 'Hybrid Cluster-based Geographical Routing Protocol to Mitigate Malicious Nodes in Mobile Ad Hoc Network, InderScience-International Journal of Ad Hoc and Ubiquitous Computing, vol. 21, no. 4, pp. 224-236. DOI:10.1504/IJAHUC.2016.076358.
20. Indumathi N et al., Impact of Fireworks Industry Safety Measures and Prevention Management System on Human Error Mitigation Using a Machine Learning Approach, Sensors, 2023, 23 (9), 4365; DOI:10.3390/s23094365.
21. Parkavi K et al., Effective Scheduling of Multi-Load Automated Guided Vehicle in Spinning Mill: A Case Study, IEEE Access, 2023, DOI:10.1109/ACCESS.2023.3236843.
22. Ran Q et al., English language teaching based on big data analytics in augmentative and alternative communication system, Springer-International Journal of Speech Technology, 2022, DOI:10.1007/s10772-022-09960-1.
23. Ngangbam PS et al., Investigation on characteristics of Monte Carlo model of single electron transistor using Orthodox Theory, Elsevier, Sustainable Energy Technologies and Assessments, Vol. 48, 2021, 101601, DOI:10.1016/j.seta.2021.101601.
24. Huidan Huang et al., Emotional intelligence for board capital on technological innovation performance of high-tech enterprises, Elsevier, Aggression and Violent Behavior, 2021, 101633, DOI:10.1016/j.avb.2021.101633.
25. Sudhakar S, et al., Cost-effective and efficient 3D human model creation and re-identification application for human digital twins, Multimedia Tools and Applications, 2021. DOI:10.1007/s11042-021-10842-y.
26. Prabhakaran N et al., Novel Collision Detection and Avoidance System for Mid-vehicle Using Offset-Based Curvilinear Motion. Wireless Personal Communication, 2021. DOI:10.1007/s11277-021-08333-2.
27. Balajee A et al., Modeling and multi-class classification of vibroarthographic signals via time domain curvilinear divergence random forest, J Ambient Intell Human Comput, 2021, DOI:10.1007/s12652-020-02869-0.
28. Omnia SN et al., An educational tool for enhanced mobile e-Learning for technical higher education using mobile devices for augmented reality, Microprocessors and Microsystems, 83, 2021, 104030, DOI:10.1016/j.micpro.2021.104030 .
29. Firas TA et al., Strategizing Low-Carbon Urban Planning through Environmental Impact Assessment by Artificial Intelligence-Driven Carbon Foot Print Forecasting, Journal of Machine and Computing, 4(4), 2024, doi: 10.53759/7669/jmc202404105.
30. Shaymaa HN, et al., Genetic Algorithms for Optimized Selection of Biodegradable Polymers in Sustainable Manufacturing Processes, Journal of Machine and Computing, 4(3), 563-574, https://doi.org/10.53759/7669/jmc202404054.
31. Hayder MAG et al., An open-source MP + CNN + BiLSTM model-based hybrid model for recognizing sign language on smartphones. Int J Syst Assur Eng Manag (2024). https://doi.org/10.1007/s13198-024-02376-x
32. Bhavana Raj K et al., Equipment Planning for an Automated Production Line Using a Cloud System, Innovations in Computer Science and Engineering. ICICSE 2022. Lecture Notes in Networks and Systems, 565, 707–717, Springer, Singapore. DOI:10.1007/978-981-19-7455-7_57.